Flexing the Electrified Meniscus: The Birth of a Jet in Electrosprays

Ioan Marginean, Lida Parvin, Linda Heffernan, and Akos Vertes*

Institute for Proteomics Technology and Applications, Department of Chemistry, The George Washington University, Washington, DC 20052

Spraying of liquids through an electrified meniscus has become a method of choice to produce ions from large biomolecules. Using mass spectrometry, the generated ions can be analyzed to provide detailed information on their composition and structure. This technique enables high-throughput protein analysis that is a prerequisite for answering the questions presented by proteomics. In this report, Taylor cone deformations are shown to play a central role in the mechanism of electrostatic spraying. Spontaneous spray current oscillations are known to exist in most electrospray regimes and affect the stream of ions introduced into the mass spectrometer. Fast time-lapse imaging of the Taylor cone throughout its evolution indicates the presence of a nodal line and standing waves on its surface. Four phases of the cone pulsation cycle (liquid accumulation, cone formation, ejection of a jet, relaxation) are established. Based on image analysis, apex velocities, curvatures, and opening angles are determined. During jet ejection, the apex velocity and the curvature exhibit singularities. Furthermore, the pulsation frequencies of the Taylor cone deformations are determined using Fourier analysis of light refraction measurements. The oscillation frequency of the electrospray current collected by the counter electrode shows close correlation to the cone deformations, providing the first direct evidence that links spray current oscillations to Taylor cone pulsation. Thus, monitoring the oscillation frequency throughout the spraying process and adjusting the spray parameters can be used to stabilize the spray. Furthermore, synchronizing the injection of ions in time-of-flight systems with the spontaneous spray oscillations may improve the signal-to-noise ratio in the collected mass spectra.

Electrified liquid interfaces are involved in natural phenomena such as lightning and rain droplet formation. The charge accumulated on the surface of water droplets might explain the excess absorption of solar radiation in the Earth's atmosphere.[1] Fallout of radioactive aerosols around clouds is facilitated by charging effects.[2] Electrohydrodynamic pumping, electroosmotic flow, electrospinning, and electrowetting are active research areas especially in connection with microfluidics and with micro- and nanoelectromechanical systems. Important technological processes such as deposition of biomaterials,[3] fuel injection, and ink-jet printing can be accomplished by the dispersion of charged liquids. Liquid metal ion sources[4] and electrospray (ES) are based on similar phenomena occurring at an electrified meniscus. In the ES ionization method, the liquid solution containing the species of interest is pumped through a metallic needle held at high voltage with respect to a counter electrode (e.g., skimmer of the mass spectrometer). The application of this ionization method for the analysis of large biomolecules[5] has revolutionized the field and laid the foundation of proteomics.[6] Charge reduction of evaporating nanodroplets is thought to be at the core of this ionization technique.[7] Fundamental ES research, however, had started long before the method proved to be useful in biomedical analysis.

In 1917, Zeleny observed for the first time the rapid electrohydrodynamic pulsation of electrified liquid surfaces.[8] He characterized the resulting spray as a function of the nature of the solvent, high voltage, and pressure of the liquid at the tip of the tube (which is linked to the flow rate in modern ES experiments). Although the nomenclature was not established at the time, he described different spraying modes including the dripping, spindle, Taylor cone, and multijet modes. Much later, a detailed description of the various spraying modes was given by Cloupeau and Prunet-Foch.[9] Zeleny also presented the first flash shadowgraphs showing images of the electrified meniscus taken at ~1.25-ms time intervals. His pictures show the cone formation, jet expulsion, its detachment, and relaxation to a droplet. These images, however, are not synchronized to the pulsation of the liquid resulting in snapshots taken at random with respect to the surface movement. Nevertheless, a few jet breakup modes, elaborately classified later as axisymmetric varicose, lateral kink, and ramified jet,[10] were also observed. Similar shadowgraphs were also obtained by Taylor,[11] who demonstrated that, in an electric field, the conical

---

* To whom correspondence should be addressed: (e-mail) vertes@gwu.edu; (phone) 202-994-2717; (fax) 202-994-5873.

(1) Geldart, D. J. W.; Chýleka, P. *J. Quant. Spectrosc. Radiat. Transfer* **2001**, *70*, 697−708.

(2) Tripathi, S. N.; Harrison, R. G. *Atmosph. Environ.* **2001**, *35*, 5817−5821.

(3) Lee, B.; Kamiya, N.; Machida, S.; Yamagata, Y.; Horie, K.; Nagamune, T. *Biomaterials* **2003**, *24*, 2045−2051.

(4) Prewett, P. D.; Mair, G. L. R. *Focused Ion Beams from Liquid Metal Ion Sources*; Wiley: New York, 1991.

(5) Fenn, J. B.; Mann, M.; Meng, C. K.; Wong, S. F.; Whitehouse, C. M. *Science* **1989**, *246*, 64−71.

(6) Cole, R. B., Ed. *Electrospray ionization mass spectrometry: fundamentals, instrumentation, and applications*; Wiley: New York, 1997.

(7) Znamenskiy, V.; Marginean, I.; Vertes, A. *J. Phys. Chem. A* **2003**, *107*, 7406−7412.

(8) Zeleny, J. *Phys. Rev.* **1917**, *10*, 1−6.

(9) Cloupeau, M.; Prunet-Foch, B. *J. Aerosol Sci.* **1994**, *25*, 1021−1036.

(10) Hartman, R. P. A.; Brunner, D. J.; Camelot, D. M. A.; Marijnissen, J. C. M.; Scarlett, B. *J. Aerosol Sci.* **2000**, *31*, 65−95.

interface between two fluids was in equilibrium for an opening angle of ~49.3°. Using shadowgraphy, Gomez and Tang proved that the charge reduction of the primary droplet proceeded through asymmetric fission.[12] Some of the droplets formed by jet breakup became highly distorted from their spherical shape, and finer jets were expelled through conical protrusions. Recently, high-speed microscopy showed the expulsion of fine jets from levitated ethylene glycol droplets charged to the Rayleigh limit.[13]

An important consequence of the pulsating liquid meniscus is the pulsation in the spray current carried by the charged droplets. Juraschek and Röllgen used spray current measurements to characterize the two pulsating axial modes and a continuous axial mode they found in their ES experiments.[14] The pulsation phenomena were explained by the imbalance between the supply and the loss of liquid in the entire cone volume (low frequencies) and in the apex region (high frequencies). In these experiments, transition between the different ES modes was induced by changing the high voltage and a sudden transition between the pulsating and continuous axial modes was noticed by monitoring the spray current. One of the most important results of ref 14 is presented in their Figure 20, which shows an excellent correlation between the ion current oscillation in the mass spectrometer and the variations in the total spray current. This observation turns out to be important in the analysis of our results because it indicates the preservation of the oscillations observed in spray current throughout the entire mass spectrometer all the way to the ion current signal recorded by the detector. The pulsation phenomena in naturally and externally pulsed ESs and some of their possible applications were recently reviewed by Wei and co-workers.[15]

This paper focuses on the most commonly utilized ES mode originating from a pulsating Taylor cone. We present time-lapse images with well-defined and known time delay between the individual frames following the fast evolution of the Taylor cone throughout the entire natural pulsation cycle. This enables us to report the first determination of the apex velocity and the time evolution of Taylor cone properties, as well as demonstrate the presence of node lines on the cone surface. Although Taylor cone pulsation[8] and spray current oscillations[16] had been reported in the literature, there was no experimental evidence linking the two phenomena. Using combined cone deformation and spray current measurements, we provide evidence that the oscillations in the spray current measurements are the direct consequence of the Taylor cone pulsation.

The last observation suggests the possibility for real-time control of the ES regime by monitoring the spray current. Combining separation methods, such as high-performance liquid chromatography (HPLC), and mass spectrometry (MS), through ES dramatically enhances the capabilities of these analytical techniques. In case of gradient elution, however, changing liquid properties during analysis frequently leads to spray instability.

Other sources of instability are related to the surface properties of the spraying capillary and to environmental conditions. Monitoring the oscillation frequency throughout the process and adjusting the spray parameters (e.g., spray voltage or liquid flow rate) through negative feedback may be used to stabilize the spray. Orthogonal extraction is commonly utilized to analyze the ions produced by a continuous source like ES with a time-of-flight (TOF) analyzer. Synchronizing the orthogonal extraction with the pulsation of the Taylor cone is expected to improve the signal-to-noise ratio for such measurements.

EXPERIMENTAL SECTION

A syringe pump (model 22, Harvard Apparatus, Holliston, MA) was used to supply aqueous methanol or acetonitrile solutions at 2 μL/min through a blunt tip stainless steel needle (model 90531, i.d. = 130 μm, o.d. = 260 μm, Hamilton Co., Reno, NV). Translation stages (F38182 and NT37-979, Edmund Industrial Optics, Barrington, NJ) allowed fine positioning of this spraying capillary in the X, Y, and Z directions. To achieve a stable axial spray, the capillary was held at 2.9 (methanol solution) or 3.1 kV (acetonitrile solution) by a regulated high-voltage power supply (model PS 350, Stanford Research Systems, Inc., Sunnyvale, CA). Because the full scale of typical current measurements was in the nanoampere range, special care was taken for electrical shielding and grounding. Air currents around the system were restricted by an enclosure.

Spray Current Measurements. A stainless steel plate counter electrode was placed at a distance of 3.0 cm from the tip of the capillary, and the current was measured by a digital oscilloscope (LC9370M, LeCroy, Chestnut Ridge, NY) at 1-MΩ input impedance. The measurements were taken through dc coupling with a bandwidth limit of 25 MHz. For each measurement, 100 000 data points were acquired at 20-kHz sampling rate and transferred through the GPIB interface to a PC computer, utilizing custom-made software based on LabVIEW 6i (National Instruments, Austin, TX) platform.

Taylor Cone Pulsation Frequency Measurements. A 0.5-mW HeNe laser (05-LLR-811, Melles Griot, Carlsbad, CA) was focused on the Taylor cone using a $f = 10$ cm focal length lens, and the refracted light was detected with a fast photodiode (Det 210, Thorlabs, Newton, NJ). The photodiode signal was recorded using the LeCroy oscilloscope through ac coupling. To assess whether the interaction of the laser with the Taylor cone influenced the prevailing physical processes, we performed current measurements while focusing the laser onto the Taylor cone. The frequency spectra (not shown) were practically identical to the spectra presented in panels c and d of Figure 4. For the methanol solution, the main frequency was 1998 $\pm$ 17 Hz, while for the acetonitrile solution, it was 2048 $\pm$ 16 Hz. On the basis of these results, we concluded that within the scope of this study the influence of the laser on the Taylor cone pulsation was negligible.

Time-Lapse Images of the Taylor Cone. In the imaging experiments, the photodiode signal was amplified 100 times (HP 465A, Hewlett-Packard, Palo Alto, CA) to provide the master trigger for a delay generator (DG535, Stanford Research Systems, Sunnyvale, CA). This device provided the variable-delay TTL level trigger for a fast camera (QICAM, QImaging, Burnaby, BC) capable of 40-μs exposure time. The individual pictures presented in this paper are averages of 100 exposures. Back illumination of

(11) Taylor, G. *Proc. R. Soc. London* **1964**, *280*, 383−397.

(12) Gomez, A.; Tang, K. *Phys. Fluids* **1994**, *6*, 404−414.

(13) Duft, D.; Achtzehn, T.; Müller, R.; Huber, B. A.; Leisner, T. *Nature* **2003**, *421*, 128.

(14) Juraschek, R.; Röllgen, F. W. *Int. J. Mass Spectrom.* **1998**, *177*, 1−15.

(15) Wei, J.; Shui, W.; Zhou, F.; Lu, Y.; Chen, K.; Xu, G.; Yang, P. *Mass Spectrom. Rev.* **2002**, *21*, 148−162.

(16) Carbonnier, F.; Rolando, C.; Saru, F.; Hapiot, P.; Pinson, J. *Rapid Commun. Mass Spectrom.* **1993**, *7*, 707−710.
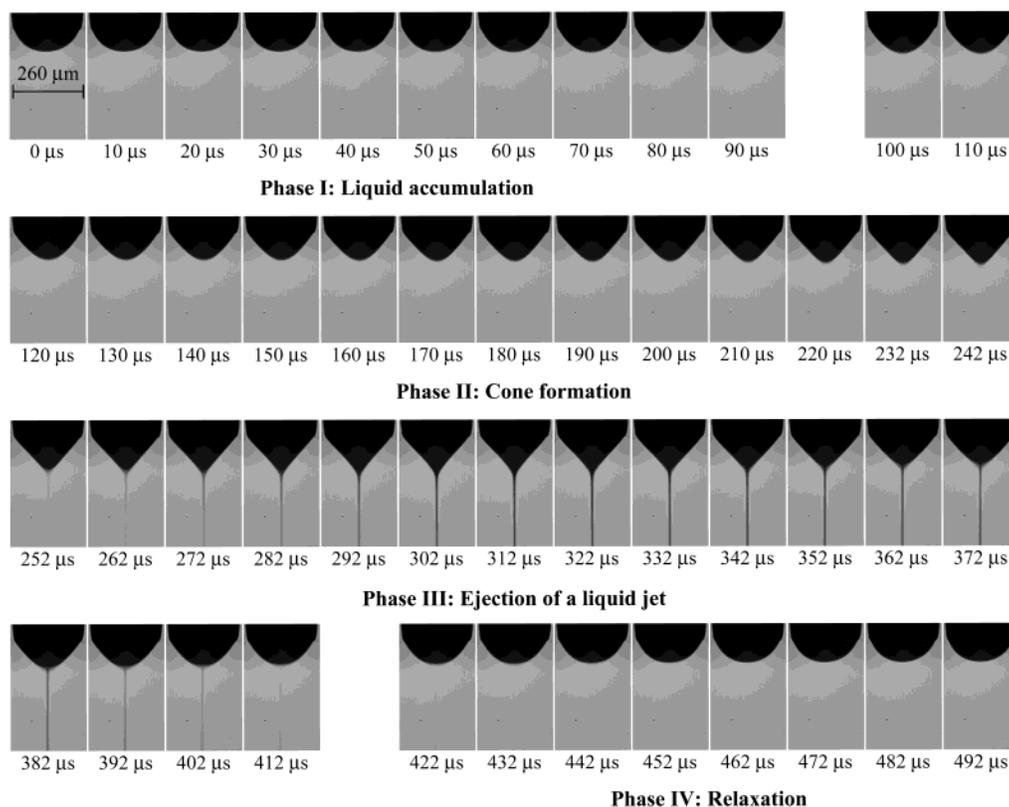
Figure 1. Time-lapse images of the pulsating Taylor cone with the four phases of the cycle. Delay time values measured from the most retracted meniscus, Δt, are shown under the individual images. Each frame is an average of 100 exposures with the same delay.

the needle tip was achieved with a continuous light source through fiber optics (model 150 Illuminator, RAM Optical Instrumentation, Inc., Irvine, CA). Adjustable magnification was accomplished by a long-distance microscope (IF3, Edmund Scientific, Barrington, NJ). The images were processed using Adobe Photoshop (Adobe, San Jose, CA) and Scion Image software packages (Scion Corp., Frederick, MD).

Materials. HPLC grade methanol and acetonitrile were purchased from Aldrich and Fischer, respectively. Deionized water (18.3 MΩ/cm) was produced using a D4631 E-pure system (Barnstead, Dubuque, IA). The results presented in this paper were obtained with 50% (v/v) aqueous solutions of methanol and acetonitrile.

RESULTS AND DISCUSSION

The pulsation of the Taylor cone has been explained as an imbalance between the electrostatic pressure and the capillary pressure at the surface of the liquid continuously supplied through the capillary.[14] Due to the electric field gradients, the charge accumulated in the liquid moves toward areas of lower potential. The migration of charges constrained by the surface and by mutual Coulomb repulsion creates a tangential stress on the liquid surface that results in the deformation of the meniscus. Due to its lower potential, the charge primarily accumulates in the apex of the meniscus resulting in the formation of the Taylor cone. Eventually, the Coulomb repulsion overcomes the surface tension forces and charged liquid is expelled from the cone as a jet. After most of the excess charge is ejected, the capillary forces regain control and the liquid surface returns to spherical shape.

To visualize the process of Taylor cone deformation and liquid ejection, time-lapse images of the meniscus were obtained. We

believe the images presented in Figure 1[22] to be the first set of sequential images of spontaneous Taylor cone deformations. As the meniscus undergoes periodic expansion and contraction, four phases can be distinguished. During phase I (0–90 μs), the liquid accumulates at the end of the capillary. The close to spherical shape of the meniscus indicates that the surface tension is dominant during this phase. In phase II (100–242 μs), the liquid surface becomes conical perceivably due to the tangential Maxwell stress. When the surface tension cannot compensate the Maxwell stress, the instability of the surface at the apex results in the ejection of a liquid jet (phase III, 252–412 μs). After phase III, a fast retraction of the liquid is observed (phase IV, 422–492 μs) and the cycle repeats. The entire pulsation cycle is shown as a movie in Supporting Information.

Panel a of Figure 2 superimposes contours of the Taylor cone cross sections in the absence of a jet obtained by processing images from phases I, II, and IV. The contours in the presence of a jet (phase III) are shown in panel b of Figure 2. Due to the nonuniform illumination and the small radial dimension of the jet, different image processing parameters were used to obtain the contours during phase III (Figure 2b). Although the presence of varicose waves on the filament emerging from the Taylor cone is established,[10] there has been no demonstration of wave phenomena on the cone itself. The stability of nodes in Figure 2a (that are the cross sections of a nodal line) proves that standing waves do exist on the cone surface. In the absence of standing waves, such fixed points could not be observed.

Deformations of the hemispherical surface due to capillary waves, can be described using the radial position of the surface, r, expanded in spherical harmonics:

$$r = \sum_l r_l^0 Y_l(\theta, \varphi = 0) \cos(\omega_l t + \epsilon_l) \qquad (1)$$

where r_l^0 is the amplitude of the lth component, ω_l and ϵ_l are the circular frequency and the phase of the lth wave, respectively. The lth normalized spherical harmonic is expressed by Legendre polynomials:

$$Y_l(\theta, \varphi = 0) = \sqrt{(2l+1)/4\pi}\, P_l(\cos\theta) \qquad (2)$$

For particular time frames, linear combinations of Legendre polynomials, $\sum_l a_l P_l(\cos\theta)$, were used to describe the shape of the meniscus using regression analysis (results not shown). In Taylor cone mode, symmetry considerations allow us to express the liquid surface position as a sum of waves with even number of nodes:

$$r =$$
$$r_0 \cos(\omega_0 t + \epsilon_0)\sqrt{\frac{1}{4\pi}} + r_2 \cos(\omega_2 t + \epsilon_2)\sqrt{\frac{5}{4\pi}} P_2(\cos\theta) +$$
$$r_4 \cos(\omega_4 t + \epsilon_4)\sqrt{\frac{9}{4\pi}} P_4(\cos\theta) + ... \quad (3)$$

The first three components of this series are in phase and are visually identifiable in Figure 2a. The first component (a breathing spherical mode) slightly increases due to liquid supply through the capillary and decreases during jet ejection. The second and third components describe the conical deformation due to the tangential stress. The third component also accounts for liquid recoil after jet ejection. Due to the change in sign of the third term, it is possible to observe the standing wave on the Taylor cone. This only happens if the corresponding frequencies are close to equal, $\omega_2 \approx \omega_4$.

To determine the velocity of the apex, its displacement is measured for the images where no jet ejection is observed. Figure 3a shows this displacement as a function of time and the corresponding velocity, $v = 0.18 \pm 0.01$ m/s, calculated from linear regression. This value is ~2 orders of magnitude smaller than the axial droplet velocities measured in ESs by phase Doppler anemometry.[17-19] For example, for sprays of 50% methanol solution at a distance of 2 mm from the tip of the needle, an axial droplet velocity of 20.2 ± 2.7 m/s was measured. Similarly, for 90% methanol solutions sprayed through a 150/510 μm i.d./o.d. needle at 4.0 kV, an axial velocity of 34.6 ± 11.8 m/s was determined.[17] The large difference between apex and droplet velocities indicates that most of the liquid acceleration takes place in the jet and after the detachment of individual droplets. Acceleration of the liquid during these phases is the result of significant potential gradient in this region and of the diminished retardation by surface tension. The initial phase of this acceleration can be observed in Figure 3a as a departure from linearity toward the end of phase II.

(17) Olumee, Z.; Callahan, J. H.; Vertes, A. *J. Phys. Chem. A* **1998**, *102*, 9154–9160.
(18) Olumee, Z.; Callahan, J. H.; Vertes, A. *Anal. Chem.* **1999**, *71*, 4111–4113.
(19) Galicia, M. C.; Gauntt, J. M.; Carney, L. M.; Nguyen, A. B.; Vertes, A. Pacifichem, Honolulu, HI, December 14–19, 2000.

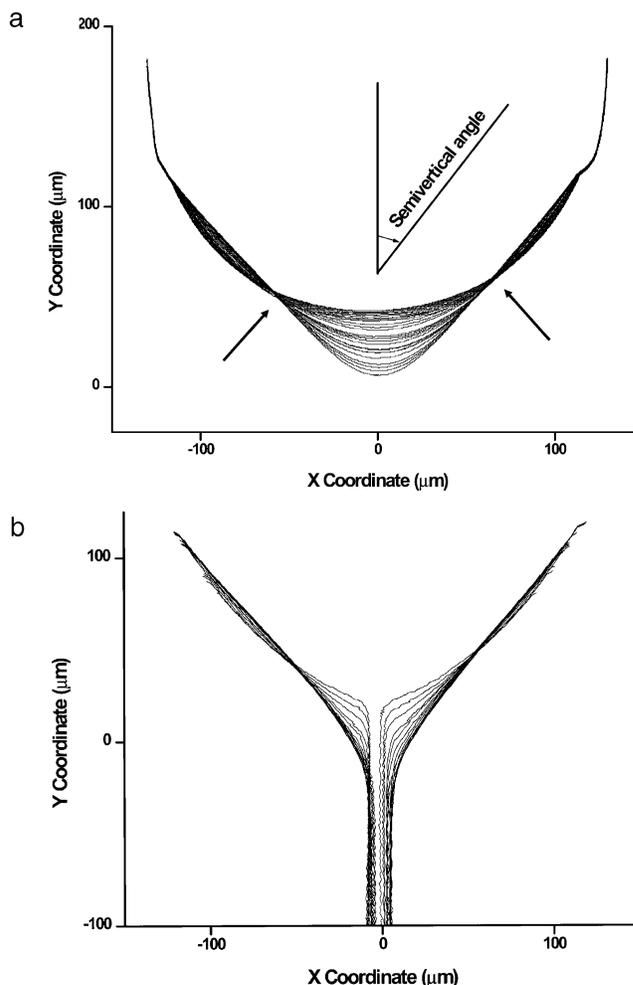**Figure 2.** Liquid surface contours clearly showing a nodal line on the Taylor cone (see arrows pointing to nodal line cross sections in panel a), proving the presence of stationary waves on its surface. Different image processing parameters were used for the two panels to emphasize the surface contours in the absence of a jet (a) and during jet ejection (b).

In phase III, the formation of a jet is observed (Figure 2b). Highly nonlinear in nature, this process cannot be described as a linear combination of capillary waves. Rather, the surface shape exhibits a singularity in the form of a jet. Figure 3b captures this process by showing the time evolution of the curvature at the liquid apex. Second-order polynomials were used to fit the contours of the liquid surface cross section, and the curvatures were calculated as the second derivatives (empty circles). In the case of images showing the emerging and extinguishing jet, the inverse of the jet radius was considered as the curvature at the apex (black circles). A sudden increase in curvature is observed right before jet ejection, and a sudden decrease in curvature indicates jet collapse.

Liquid jet ejection may be observed under a wide range of fluid flow conditions (collapsing cavities, inertial focusing, and surface waves at a wall).[20,21] Scaling law-type solutions to the flow equations dominated by inertia and surface tension have been found to

(20) Longuet-Higgins, M. S., Oguz, H. N. *Philos. Trans. R. Soc. London A* **1997**, *355*, 625–639.
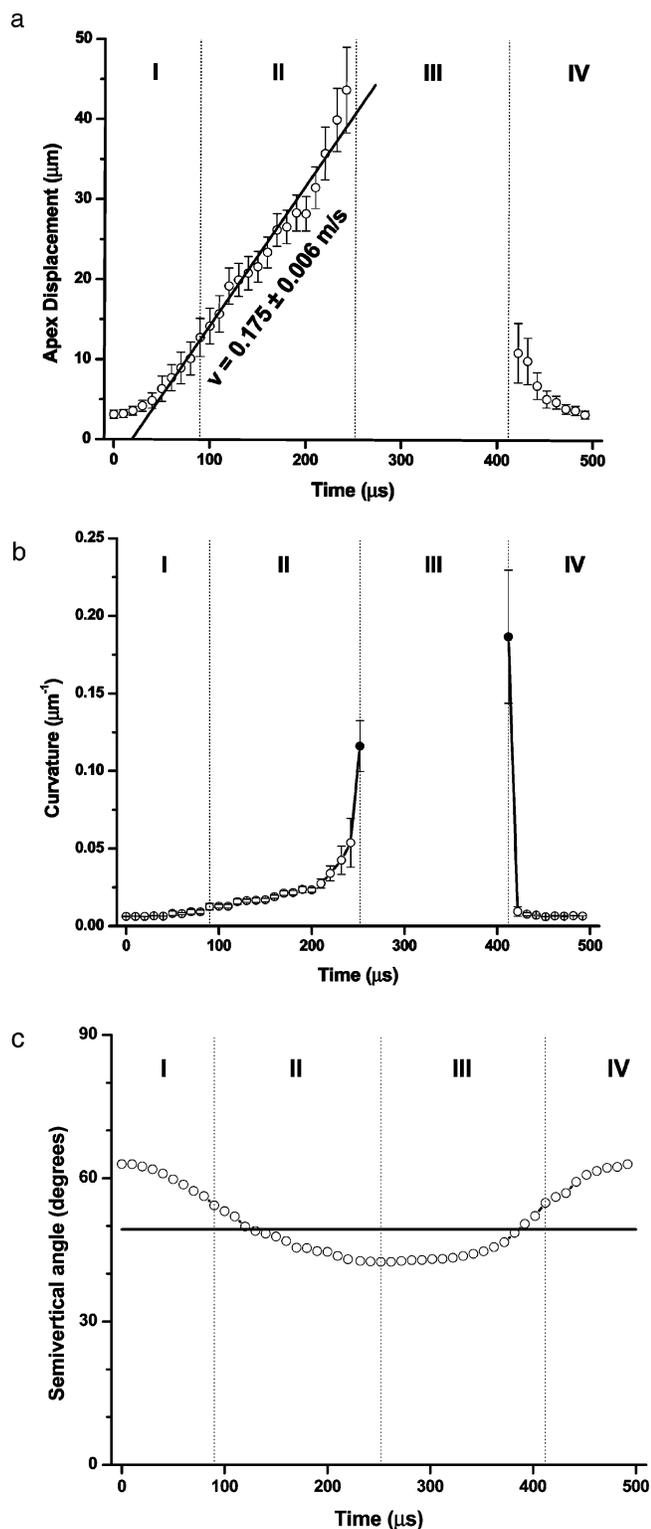(21) Zeff, B. W., Kleber, B., Fineberg, J., Lathrop, D. P. *Nature* **2000**, *403*, 401–404.
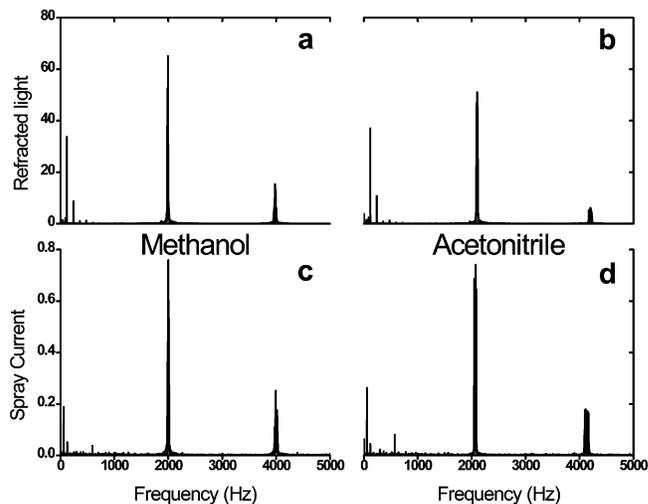
Figure 4. Fourier transform amplitude spectra of Taylor cone deformation (a and b panels) and spray current data (c and d panels) obtained at 2 μL/min flow rate for 50% methanol at 2900 V (a and c panels) and 50% acetonitrile at 3100 V (b and d panels) showing direct correlation between Taylor cone pulsation and spray current oscillation.

Figure 3. Taylor cone evolution in time: (a) apex displacement, (b) surface curvature at the apex, and (c) opening angle derived from the angle of tangent at the nodes.

accurately describe the shape of the liquid surface at times close to jet ejection. According to these solutions, during the time leading up to the ejection the velocity of the apex can be expressed as

$$v \propto (t_d - t)^{\alpha - 1} \tag{4}$$

where t_d is the time of jet detachment and $\alpha = {}^2/_3$. A detachment time of 360 μs was obtained by fitting the nonlinear portion of the apex velocity data with eq 4. This indicates that the jet detachment takes place relatively late during phase III, corroborating that the recoil is much faster than the jet formation. The divergence of v before jet detachment can help to explain the large difference found between measured values of the apex velocity before jet formation (phase II) and the velocity of the droplets after jet breakup. Individual images (not shown) captured shortly before jet ejection and during the jet detachment show low optical density in the apex region. The rapid movement of the apex, on a time scale shorter than the exposure time of the camera, might explain this low optical density.

The two nodes on the contours in Figure 2a enable the determination of the angle of tangent lines, ζ, that can be compared for the entire sequence of images. Figure 3c presents the angles complementary to ζ that oscillate around Taylor's theoretical value, 49.3°, shown as a horizontal line. The initial slow time evolution of the angle indicates a gradual charging process (20−232 μs), followed by jet ejection at almost constant opening angle (45.5 ± 3.8°). The subsequent angle increase is faster (352−472 μs) and implies that even before the jet ejection is over the surface tension rapidly regains control of the process. The asymmetry of the plot reflects an asymmetric charging-discharging cycle.

To determine the characteristic frequencies of the capillary waves (e.g., ω_2 and ω_4), Taylor cone deformations were followed through monitoring the refraction of a HeNe laser beam on the liquid cone. Figure 4a shows the Fourier spectrum of the signal proportional to the refracted light intensity for a representative measurement conducted on 50% (v/v) methanol solution. The spectrum shows a single frequency for the deformations, $\omega_2 = \omega_4 = 1993 \pm 17$ Hz, and its second harmonic. The peaks appearing in the low-frequency domain are interfering harmonics of the 60-Hz line voltage. Similar data for 50% (v/v) acetonitrile solution in Figure 4b indicate a change in the oscillation frequency, $\omega_2 = \omega_4$

= 2101 ± 20 Hz. The dc components in all Fourier spectra were omitted because their large amplitudes would render the ac components unnoticeable.

To explore the relationship between Taylor cone deformations and oscillations in the spray current, we measured the current on the counter electrode. Fourier analysis of the current data provided well-defined oscillation frequencies. Figure 4c shows a representative frequency spectrum for 50% (v/v) methanol solution. A single peak at 2003 ± 15 Hz and its second harmonic are observed in the high-frequency domain. The low-frequency domain contains only weak peaks corresponding to the interfering 60-Hz component and its harmonics. Remarkably, the frequency of current oscillations and the frequency of Taylor cone deformations are the same within experimental error. Similar measurements were performed for 50% (v/v) acetonitrile solution, and the Fourier spectrum is presented in Figure 4d. The high voltage was slightly increased for these measurements to maintain the spray in the Taylor cone regime. The frequency spectrum exhibited a peak at 2059 ± 20 Hz and its second harmonic. Although less accurately than the methanol measurements, these results also show agreement between Taylor cone deformation and spray current oscillation frequencies.

In addition to contributing to our understanding of the ES process, Fourier analysis of the spray current provides rich information on the spraying mode and its stability and can be used for real-time control of the ES regime. One might argue that simple monitoring of the spray current would be equally effective to using Fourier analysis of the spray current for stability control under conditions of changing liquid composition. Indeed, the spray current and its Fourier spectrum contain the same information. Minor changes in oscillation frequency, however, are expressed much more clearly in the Fourier spectrum. In fact, short of using Fourier analysis, it is hard to notice a change in spray current

oscillation frequency for example, from 2.0 kHz to 1.7 kHz. This type of frequency shift is easily picked up in the Fourier spectrum and can be used as an early indication of changes in spray stability. This could be especially important in HPLC−MS when gradient elution is used. Synchronization of orthogonal extraction in TOF-MS with the Taylor cone pulsation might also improve the signal-to-noise ratio of the measurements. This notion is supported by the combination of spray current oscillation results in this paper and the oscillations observed in the ion current (i.e., the analytical signal) in ref 14.

It should also be noted that the rapid pulsation in ES phenomena can have significant implications in case of fast-scanning mass spectrometers. If the scanning rate is comparable to the rate of spray current variations, large variations in spectral peak intensities can result. Conversely, synchronizing the scanning of the mass spectrometer to the spray pulsation may improve the stability of the analytical signal.

SUPPORTING INFORMATION AVAILABLE

A movie showing the Taylor cone evolution during one cycle of its natural pulsation. This material is available free of charge via the Internet at http://pubs.acs.org.